Geophysical Prospecting

EAGE EUROPEAN ASSOCIATION OF GEOSCIENTISTS & ENGINEERS

Geophysical Prospecting, 2013, **61** (**Suppl. 1**), 300–316 doi: 10.1111/1365-2478.12012

Pseudo-remote reference processing of magnetotelluric data: a fast and efficient data acquisition scheme for local arrays

G. Muñoz and O. Ritter

Helmholtz Centre Potsdam, German Research Centre for Geosciences GFZ Telegrafenberg, 14473 Potsdam, Germany

Received June 2012, revision accepted October 2012

ABSTRACT

The basic physical properties of the magnetic source field, namely its homogeneity and spatial coherence, have been used for a variety of magnetotelluric processing techniques including remote reference processing. In the present work we propose a data acquisition and processing technique for a large number of stations distributed over a localized area ideally on a grid. For pseudo-remote reference processing it is necessary to use the following station setup: five-component MT data are only measured at some sites (base stations) while at the majority of sites (local stations) only the electric and vertical magnetic fields are recorded. The impedance tensor and vertical magnetic transfer functions at each local station are computed by assigning the magnetic fields of a base station to the local station as if they had been measured there. This approach can lead to biased or erroneous estimates of local transfer functions at stations in the vicinity of strong conductivity contrasts that can be corrected using the interstation transfer functions between the horizontal magnetic fields measured at the base station(s).

We test this approach with a data set collected in the vicinity of the Groß Schönebeck geothermal test site. Magnetotelluric data were collected at 146 local and 5 base stations distributed over an approximately 5 km × 25 km wide grid with site spacing ranging from 500 m × 500 m to 1000 m × 1000 m in the frequency range 128–0.001Hz. The obtained pseudo-remote reference transfer functions are generally smooth and consistent and conductivity models obtained from 2D inversion of the data are in agreement with previous conductivity models from the study area.

Key words: Pseudo-remote, Magnetotelluric, Transfer function.

INTRODUCTION

The development of three-dimensional (3D) inversion codes for magnetotelluric (MT) data has become feasible over the last couple of years with several codes having been made available either freely or commercially (e.g., Mackie, Rodi and Watts 2001; Siripunvaraporn *et al*. 2005; Egbert and Kelbert 2012). Parallelized codes together with advances in cluster computing have allowed using bigger meshes and data sets. One of the main difficulties when planning a 3D experiment in comparison with the more traditional two-dimensional (2D) profiles is to achieve good site coverage, as this can dramatically increase the time and costs of field experiments. Here we present a data acquisition scheme that can help shorten the setup time of the MT stations, thereby reducing the overall length of the field experiment and allowing for an optimized use of resources. Based on the physical properties of the magnetic source field – its homogeneity and spatial coherence – we propose measuring horizontal magnetic fields only at some base stations, while the spatially more rapidly changing electric and vertical magnetic field components are sampled at

Email: gmunoz@gfz-potsdam.de

all points of the measurement grid. This way, the impedance tensor and vertical magnetic transfer functions at each station are constructed as a combination of locally measured fields together with the horizontal magnetic fields from one (or several) of the base stations. Obviously, this approach requires highly accurate synchronization between instruments, which is possible with modern equipment. Using this approach in the vicinity of the Groß Schönebeck geothermal test site in the north eastern German Basin, we were able to install up to nine stations per day working with a team of six people and complete a measuring grid of 151 stations with a recording time of 3 days per site in just 25 days including mobilization and demobilization.

THEORETICAL BACKGROUND

The spatial coherence of the magnetic source field (Zweier and Morrison, 1972) has been widely used for a variety of processing techniques such as the remote reference technique (Goubau, Gamble and Clarke 1978), electromagnetic array profiling (EMAP, Torres-Verdin and Bostick 1992) or to improve data quality in the audio-magnetotellurics (AMT) dead band (Garcia and Jones 2005). We propose the acquisition of a large number of stations distributed over a relatively localized area, ideally on a grid. For this proposed approach, 'normal' five-component MT stations are only measured at some sites (base stations), for instance in the corners and the centre of a grid, while for the rest of sites (local stations) only the 'local' fields, i.e., the electric and vertical magnetic fields are measured. The full-impedance tensor and vertical magnetic transfer functions at each of the local stations are computed by assigning the magnetic fields measured at one of the base stations to the local station as if they had been measured there. This approach, which was described as the pseudo-remote reference by Ritter, Junge and Dawes (1998), can lead to biased or erroneous estimates of local transfer functions at stations in the vicinity of strong conductivity contrasts. Here, large secondary magnetic fields are superimposed on the magnetic source fields that are not accounted for. Figure 1 shows an example of local and pseudo-remote transfer functions for a synthetic model consisting in a 100 Ωm half-space with a 1 Ωm anomaly embedded. The synthetic responses for this and all subsequent models were calculated using the 3D forward modelling code of Mackie, Madden and Wannamaker (1993). If the base station is chosen far from the conductive anomaly (base station 109), local and pseudo-remote transfer functions are similar for stations located at some distance from the conductor (e.g., site 252 in Fig. 1) but the pseudo-remote transfer functions are biased for stations located above or close to the conductor (e.g., sites 144 and 94 in Fig. 1).

A measure for the homogeneity of the source fields in the measurement area can be obtained from the inter-station transfer functions (ITF), which connect the horizontal magnetic fields between any two sites (for these and all subsequent equations, dependence on frequency is assumed):

$$\begin{aligned} \mathbf{B}_1 &= \mathbf{T}_{1-2}\mathbf{B}_2, \\ \begin{pmatrix} B_x \\ B_y \end{pmatrix}_1 &= \begin{pmatrix} T_{xx} & T_{xy} \\ T_{yx} & T_{yy} \end{pmatrix} \begin{pmatrix} B_x \\ B_y \end{pmatrix}_2 . \end{aligned} \tag{1}$$

For uniform field sources and in absence of lateral conductivity anomalies, $\mathbf{T} = \mathbf{I}$ for all frequencies. The presence of lateral conductivity changes gives rise to anomalous horizontal magnetic fields that cause $\mathbf{T}$ to be complex valued and frequency dependent (Larsen *et al*. 1996). The observed ITFs of densely spaced sites, however, are often close to unity (Ritter *et al*. 1998). Figure 2 shows the ITF between each of the 5 base stations (109, 209, 309, 409 and 509) with respect to the base located in the SW corner (station 109). All station pairs show the ITF very close to unity, except for the central base station, which shows larger deviations from unity. Obviously stations located near the centre of the grid (i.e., in the vicinity of the conductive body) can be severely biased by the pseudo-remote approach.

The impedance tensor $\mathbf{Z}$ is calculated from electric and magnetic fields in the frequency domain:

$$\begin{pmatrix} E_x \\ E_y \end{pmatrix} = \begin{pmatrix} Z_{xx} & Z_{xy} \\ Z_{yx} & Z_{yy} \end{pmatrix} \begin{pmatrix} B_x \\ B_y \end{pmatrix}. \tag{2}$$

For the local electric ($\mathbf{E}_L$) and the base magnetic ($\mathbf{B}_B$) fields, the impedance tensor assumes the pseudo-remote impedance tensor form:

$$\begin{aligned} \mathbf{E}_\mathrm{L} &= \mathbf{Z}_\mathrm{L}\mathbf{B}_\mathrm{L} \\ \mathbf{E}_\mathrm{L} &= \mathbf{Z}_\mathrm{L}\mathbf{T}_{\mathrm{B-L}}\mathbf{B}_\mathrm{B} = \mathbf{Z}_{\mathrm{pseudoRR}}\mathbf{B}_\mathrm{B} \\ \mathbf{Z}_{\mathrm{pseudoRR}} &= \mathbf{Z}_\mathrm{L}\mathbf{T}_{\mathrm{B-L}} = \begin{pmatrix} Z_{xx} & Z_{xy} \\ Z_{yx} & Z_{yy} \end{pmatrix} \begin{pmatrix} T_{xx} & T_{xy} \\ T_{yx} & T_{yy} \end{pmatrix} \\ &= \begin{pmatrix} Z_{xx}T_{xx} + Z_{xy}T_{yx} & Z_{xx}T_{xy} + Z_{xy}T_{yy} \\ Z_{yx}T_{xx} + Z_{yy}T_{yx} & Z_{yx}T_{xy} + Z_{yy}T_{yy} \end{pmatrix}. \end{aligned} \tag{3}$$

The off-diagonal components of the pseudo-remote impedance tensor consist in two terms: one multiplying a main diagonal component of the local impedance tensor with an off-diagonal component of the ITF, the other one multiplying an off-diagonal component of the impedance tensor with a main diagonal component of the ITF. For 1D or

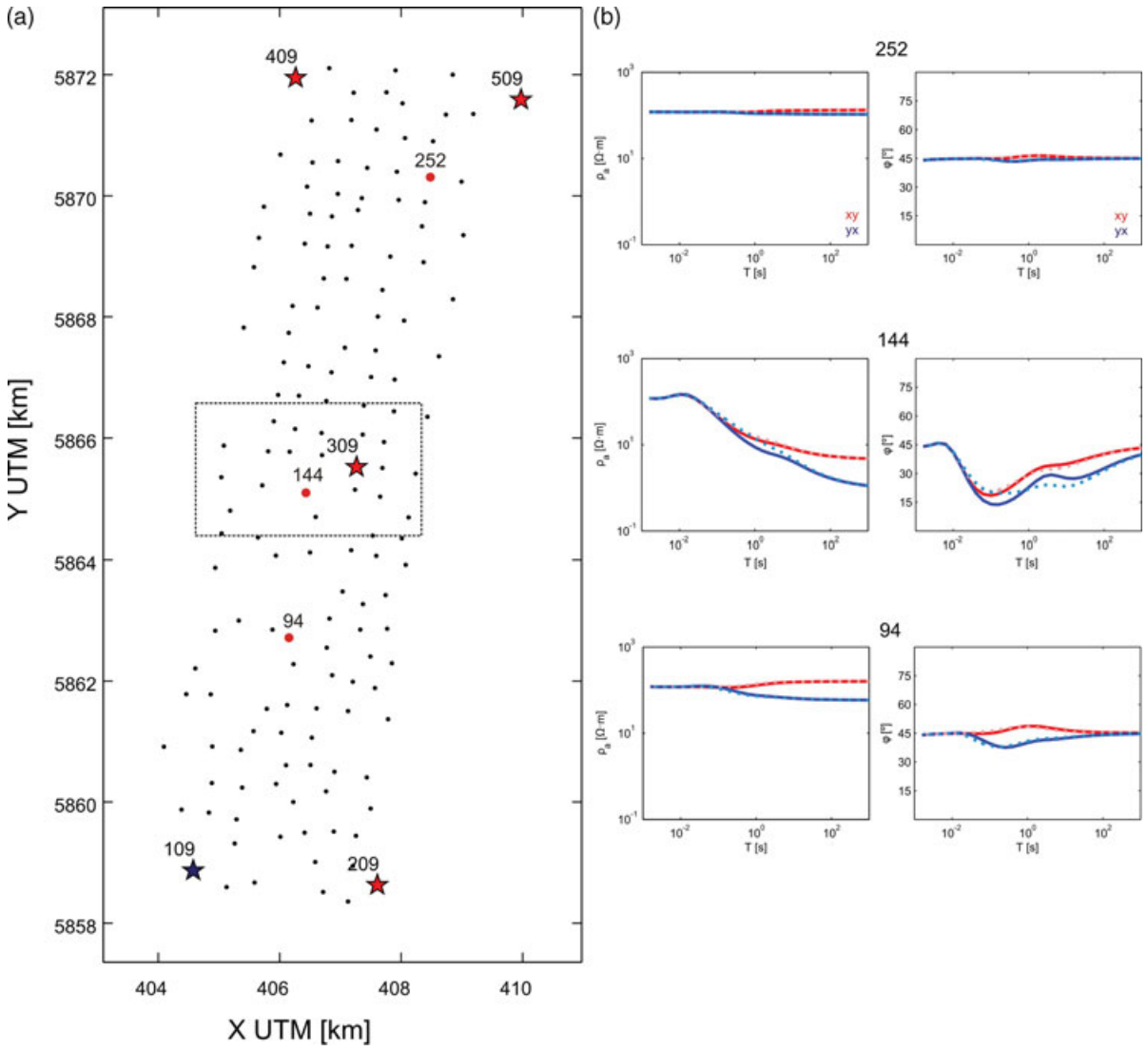

Figure 1 a) Location map of local (dots) and base (asterisks) stations for synthetic tests and to compare local site responses with pseudo-remote transfer functions. The base station used for the pseudo-remote approach is marked in blue (site 109). Red dots represent stations for which the transfer functions are shown (94, 144 and 252). The black dashed line in the map marks the outline of a high-conductivity anomaly (1 Ωm), which extends from 900–3600 m in depth. b) Comparison of the synthetic responses for three selected sites. Solid lines represent transfer functions of the local stations and dashed lines the pseudo-remote transfer functions.

2D distributions of the electrical conductivity the main diagonal components of **Z** are zero and even in the presence of 3D structures they are usually significantly smaller than the off-diagonal components. Also, **T** will be close to unity and, as a first approximation, we can write the off-diagonal components of the pseudo-remote impedance tensor as:

$$\begin{aligned} Z_{pRR,xy} &\approx Z_{xy} T_{yy} \\ Z_{pRR,yx} &\approx Z_{yx} T_{xx}. \end{aligned} \tag{4}$$

From equation (4) we observe that the main diagonal components of the inter-station transfer functions provide an estimate for the difference between off-diagonal components of local and pseudo-remote impedance tensor components.

A similar correction can be applied for the vertical magnetic transfer functions, which relate the vertical component of the magnetic field to the horizontal components according to:

$$B_z = \begin{pmatrix} T_x & T_y \end{pmatrix} \begin{pmatrix} B_x \\ B_y \end{pmatrix}. \tag{5}$$

Expressing the horizontal magnetic fields of the local station in terms of the ITF and the fields of the base station, we get the following expression for the pseudo-remote estimate of

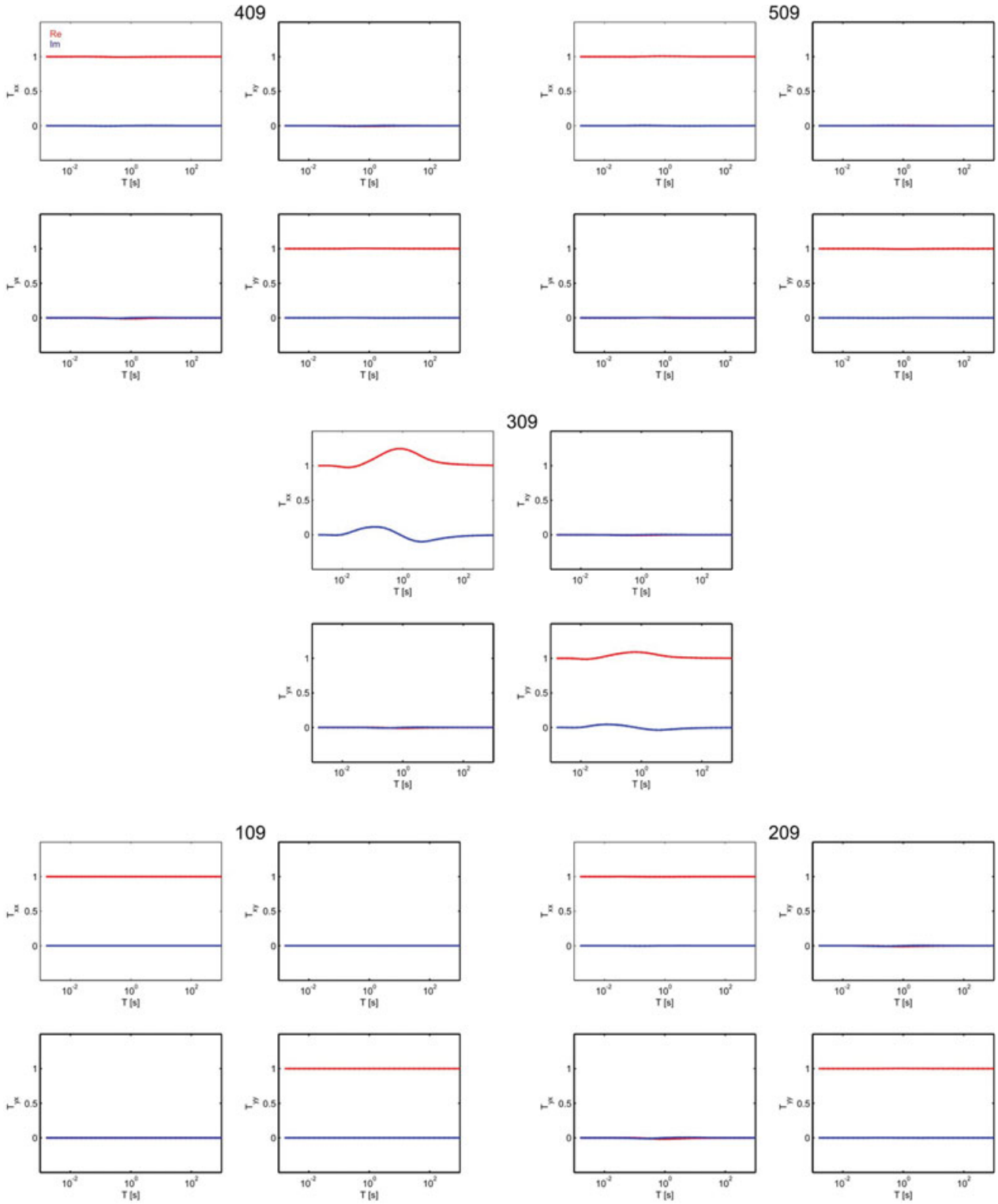

Figure 2 Interstation transfer functions (ITF) between each of the base stations and base station 109. The red line represents the real part of the ITF and the blue line the imaginary part. For all base stations located in the grid corners the ITF is very close to the identity matrix **I** (for the base station 109 it is exactly **I**, as it is the ITF between the station and itself). For station 309, located in the middle of the grid and above the conductive anomaly, the ITF shows significant deviation from **I** especially for the diagonal components.

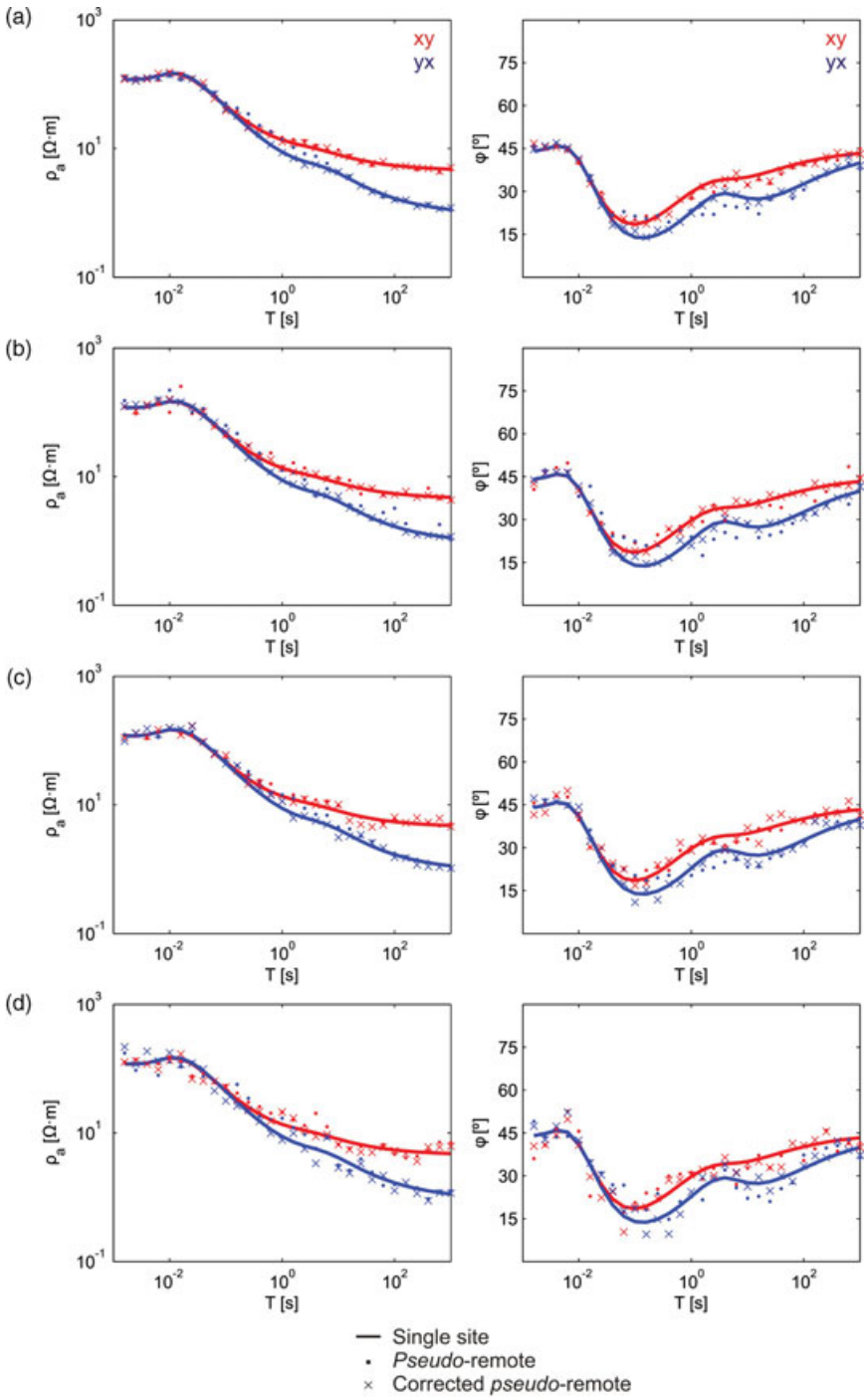

Figure 3 Comparison of the apparent resistivity and phase curves for station 144 located above the conductive anomaly (Fig. 1) under different noise conditions. The solid lines represent local transfer functions without noise. The dots represent pseudo-remote transfer functions using station 109 as a base station and crosses represent corrected transfer functions according to equations (4) and (7) and estimated ITFs according to equation (8). For a) all the fields were contaminated with 3% Gaussian noise, for b) the fields at base station 109 were additionally contaminated with 10% Gaussian noise and for c) base stations 209, 309, 409 and 509 were contaminated with 10% Gaussian noise. Finally, for d) all fields were subjected to 10% Gaussian noise. For case a) the corrected transfer functions recover the local undistorted transfer functions satisfactorily. In case b) the corrected transfer function recovers the local transfer function and even improves the quality of the pseudo-random transfer function, which is more distorted due to the additional noise at base station 109. For case c), in spite of the additional noise at the base stations used for estimating the ITF, the corrected transfer functions reproduce satisfactorily the local undistorted transfer function. For case d), however, the noisy fields cause scattering in both the pseudo-remote and corrected transfer functions, which makes it difficult to recognize to what extend the local transfer functions are recovered.

the vertical magnetic transfer function:

$$B_z = (T_x \quad T_y)\begin{pmatrix} B_x \\ B_y \end{pmatrix}_L = (T_x \quad T_y)\begin{pmatrix} T_{xx} & T_{xy} \\ T_{yx} & T_{yy} \end{pmatrix}\begin{pmatrix} B_x \\ B_y \end{pmatrix}_B$$
$$= (T_x \cdot T_{xx} + T_y T_{yx} \quad T_x \cdot T_{xy} + T_y \cdot T_{yy})\begin{pmatrix} B_x \\ B_y \end{pmatrix}_B. \qquad (6)$$

Using the same approximations for 2D conditions as before we obtain:

$$T_{pRR,x} \approx T_x T_{xx}$$
$$T_{pRR,y} \approx T_y T_{yy}. \qquad (7)$$

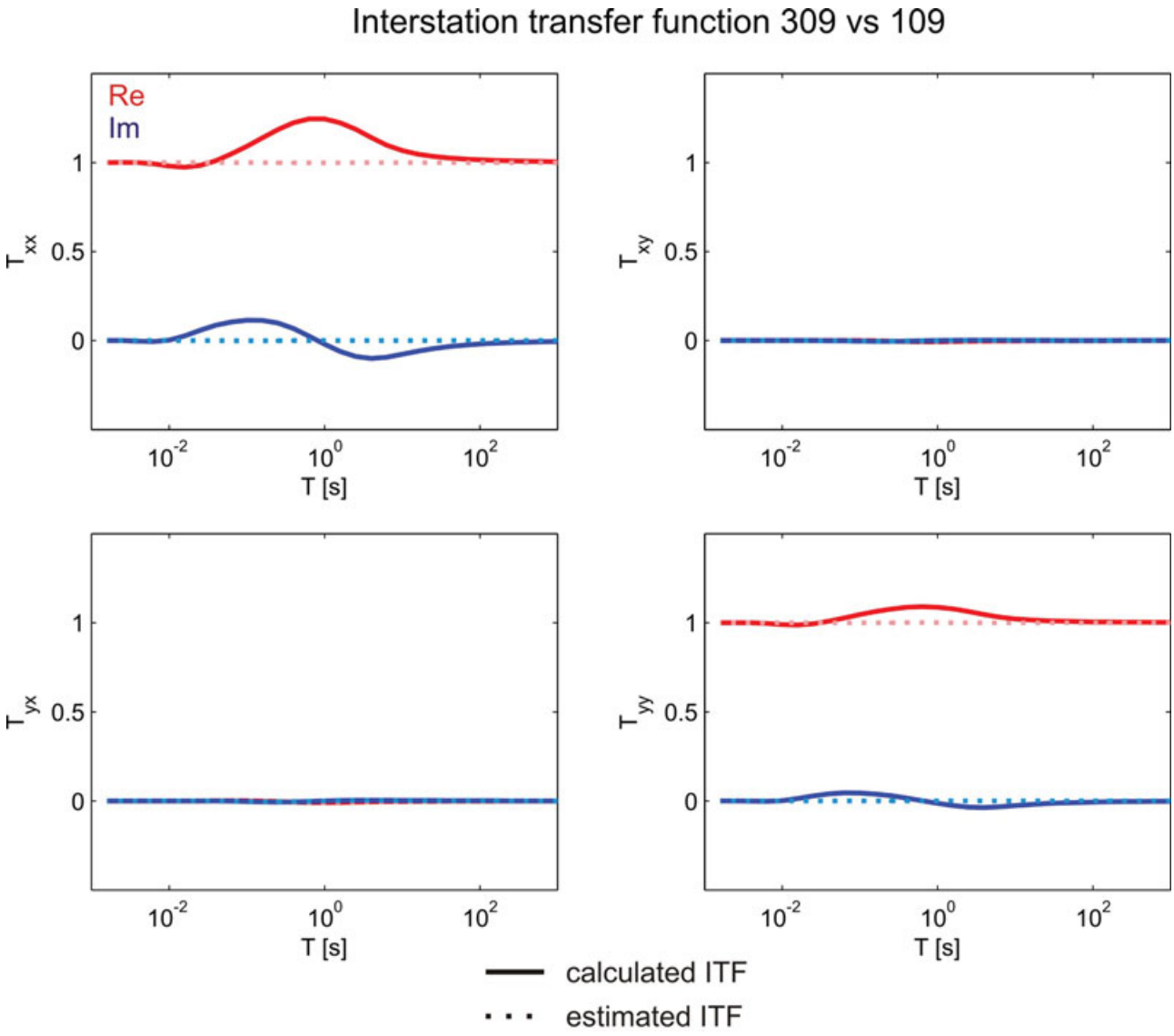

Figure 4 Interstation transfer function for the station pair 309–109. Solid lines represent the true ITF and dashed lines the ITF estimated according to equation (8) but excluding station 309 (i.e., treating station 309 as a local station). The estimated ITF is very close to unity, as it was calculated as a linear combination of ITFs ($\mathbf{T}_{109–209}$, $\mathbf{T}_{109–409}$ and $\mathbf{T}_{109–509}$), which are not sensitive to the central conductive anomaly and therefore very close to unity. The calculated ITF differs from unity due to the non-homogeneous fields produced by the conductive anomaly.

In general and for the acquisition setup described above, we do not know the values of the ITF and therefore it is not possible to apply the corrections. What is possible, however, is to check the homogeneity of the horizontal magnetic fields in the survey area by means of the ITF between all base stations. If a sufficient number of base stations are distributed evenly across the measurement grid and if all combinations of T between these sites are close to unity, we can conclude that the source field is homogeneous and that the pseudo-remote reference approach will not produce a significant bias.

From closer inspection of equations (4) and (7) we can identify a rule of thumb to estimate the magnitude of the bias. The relationship between the pseudo-remote and the local transfer functions (i.e., the bias) is proportional to the magnitude of the main diagonal components of the ITF. Therefore, to ensure biases below 10%, for example, ITFs between all base stations should also deviate from unity by less than 10% (i.e., vary between 0.9–1.1 for the real parts of the main diagonal components and between −0.1 and 0.1 for all other components).

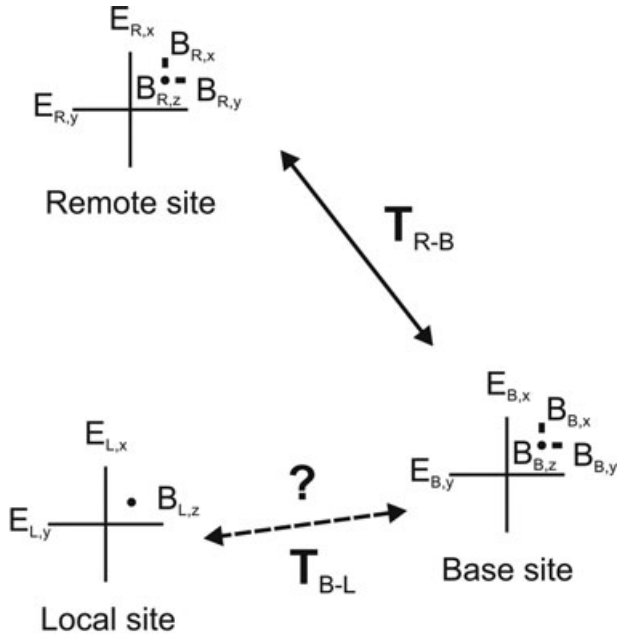

Figure 5 Schematic experimental setup for an expanded pseudo-remote/remote approach: horizontal electrical vertical magnetic fields are measured locally, while five-component electromagnetic field data (two horizontal electric field components and three magnetic field components) are measured at the base and remote stations. The interstation transfer function between local and base stations ($\boldsymbol{T}_{\mathrm{B-L}}$) is unknown; the ITF between base and remote stations ($\boldsymbol{T}_{\mathrm{R-B}}$) is part of the calculation of the remote reference transfer functions.

To apply the corrections of equations (4) and (7) we can estimate ITFs between local and base stations as a weighted average of the ITF between the base stations, which can be calculated because records of the horizontal magnetic fields are available at all base stations:

$$\mathbf{T}_{\mathrm{B_j-L}} = \frac{1}{\sum_{i}^{N} \alpha_i} \sum_{i}^{N} \alpha_i \mathbf{T}_{\mathrm{B_i-B_j}}, \tag{8}$$

where $\mathbf{T}_{\mathrm{Bj-L}}$ is the ITF between a local station and the j-th base station, $\mathbf{T}_{\mathrm{Bi-Bj}}$ is the ITF between the i-th and the j-th base stations and α_{i} is a weighting factor for the i-th base station. For the weight α_{i}, we can choose, for instance, the inverse of the distance between a local station and the i-th base station squared, thereby assigning a greater weight to the ITF of the base stations closer to the local station and a smaller weight to the ITF of base stations located farther away. Figure 3 demonstrates this approach under different noise conditions. The synthetic responses for the test model (1 Ωm conductive body embedded in a 100 Ωm resistive half-space) are shown for station 144 located above the conductive anomaly. The solid lines represent local transfer functions without noise. The dots represent pseudo-remote transfer functions using station 109 as the base station; the crosses represent corrected transfer functions according to equations (4) and (7) and estimated ITFs according to equation (8). For Fig. 3(a) all the fields were contaminated with 3% Gaussian noise, for Fig. 3(b) the fields at base station 109 were additionally contaminated with 10% Gaussian noise and for Fig. 3(c) base stations 209, 309, 409 and 509 were contaminated with 10% Gaussian noise. Finally for Fig. 3(d) all fields were subjected to 10% Gaussian noise. For cases a), b) and c), the corrected transfer functions recover the local undistorted transfer functions satisfactorily. In case b), the quality of the pseudo-random transfer function is improved, although it is more distorted due to the additional noise at the base station. For case d), however, the noisy fields cause scattering in both the pseudo-remote and the corrected transfer functions, which makes it difficult to recognize to what extend the local transfer functions are recovered. In presence of strong noise, the correction of the pseudo-remote transfer functions would probably fail but in this case the local transfer functions are also severely reduced in quality.

It should be noted that the ITF obtained from equation (8) represents an estimated value of the true ITF, which depends on the resistivity contrasts between local and all base stations and not only, as equation (8) implies, on the resistivity contrasts between the base stations. Figure 4 shows true ITFs between stations 309–109 in comparison with the ITF estimated according to equation (8) but excluding 309 (i.e., treating station 309 as a local site). In this case the estimated ITF differs strongly from the true one. Closer inspection of Fig. 2 reveals that the ITFs of the station pairs 109, 209, 409 and 509 with respect to 109 are all close to unity as they are all located far away from the conductive anomaly at the centre of the grid. ITF $\mathbf{T}_{309-109}$ estimated according to equation (8) is also close to unity, while the true $\mathbf{T}_{309-109}$ shows deviations from unity as a response to the conductive anomaly located beneath station 309. To minimize bias produced by estimating the ITF according to equation (8), the base stations should be sensitive to all major resistivity contrasts in the study area. This can be tested by estimating the ITF of each base station as if it were a local station using equation (8) and comparing the estimated transfer function with the measured one.

In the presence of galvanic distortion, the relationship between the observed and the local impedance tensor is expressed as:

$$Z_{\mathrm{L}}^{\mathrm{observed}} = \mathbf{C} \cdot \mathbf{Z}_{\mathrm{L}}. \tag{9}$$

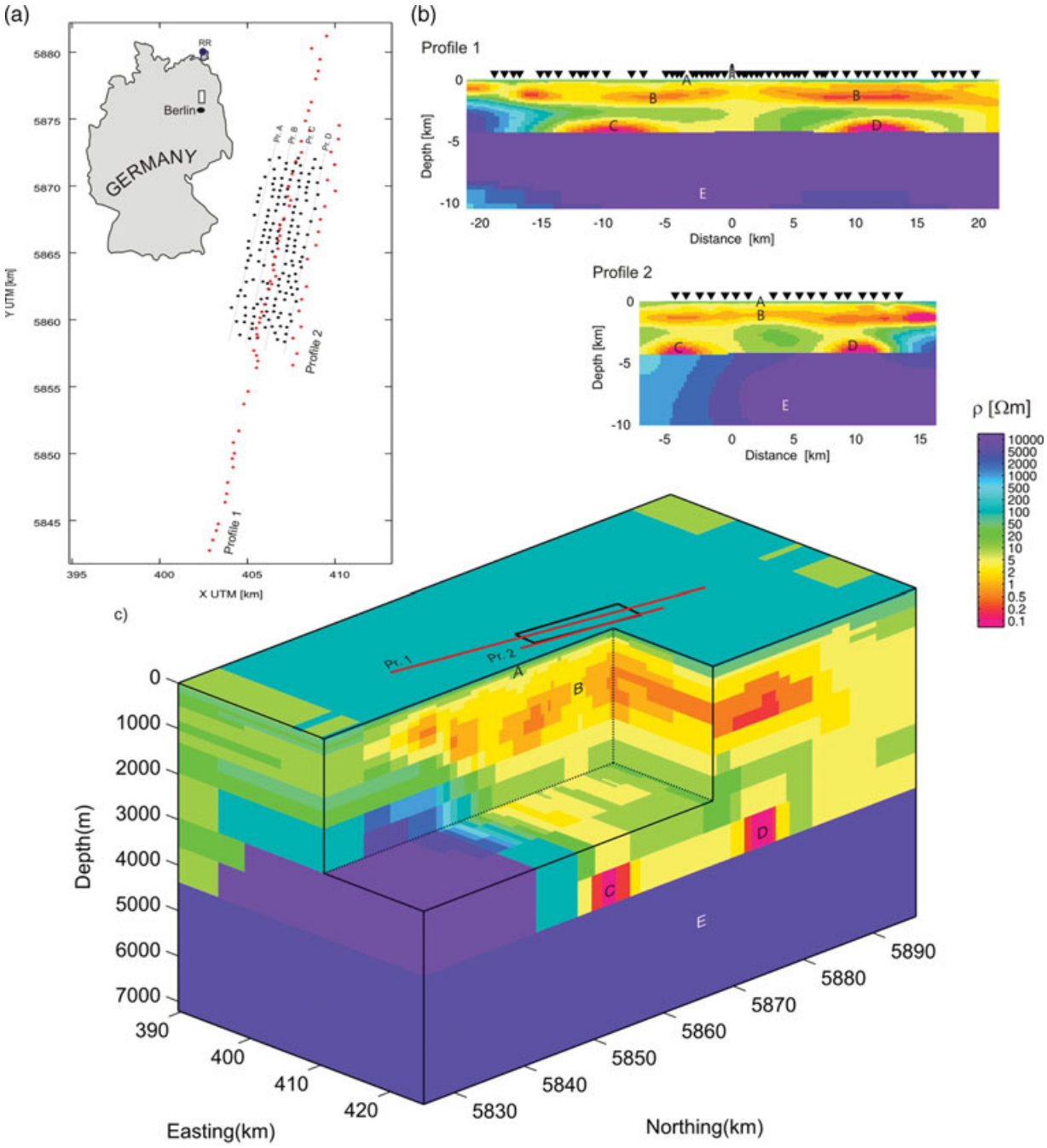

Figure 6 a) Location map of the grid stations (black dots) and two existing MT profiles (red dots; Muñoz *et al*. 2010b). The inset map of Germany indicates the location of the study area (grey rectangle) and the remote reference station (blue circle) and the thin black dotted lines indicate the position of the four profiles (A–D) later used for 2D inversion of the magnetotelluric data. b) Electrical conductivity models obtained from 2D inversion of magnetotelluric data along the two existing profiles in the area of the Groß Schönebeck geothermal test site (Modified after Muñoz *et al*. 2010b). Electrical conductivity features include: moderate conductivity layer (~50 Ωm) associated with shallow sediments (A), a high-conductivity layer (<5 Ωm) with lateral heterogeneities ranging from 1000–3000 m depth corresponding to Bundsandstein sediments (B), very high-conductivity anomalies (<1 Ωm) at the reservoir (Rotliegend) level (ca. 4500 m depth) possibly associated with a fractured overlaying evaporitic layer (C and D) and a high-resistive (>5000 Ωm) basin floor (E). c) Simplified 3D conductivity model obtained from inter- and extrapolation of the 2D models used for synthetic tests.

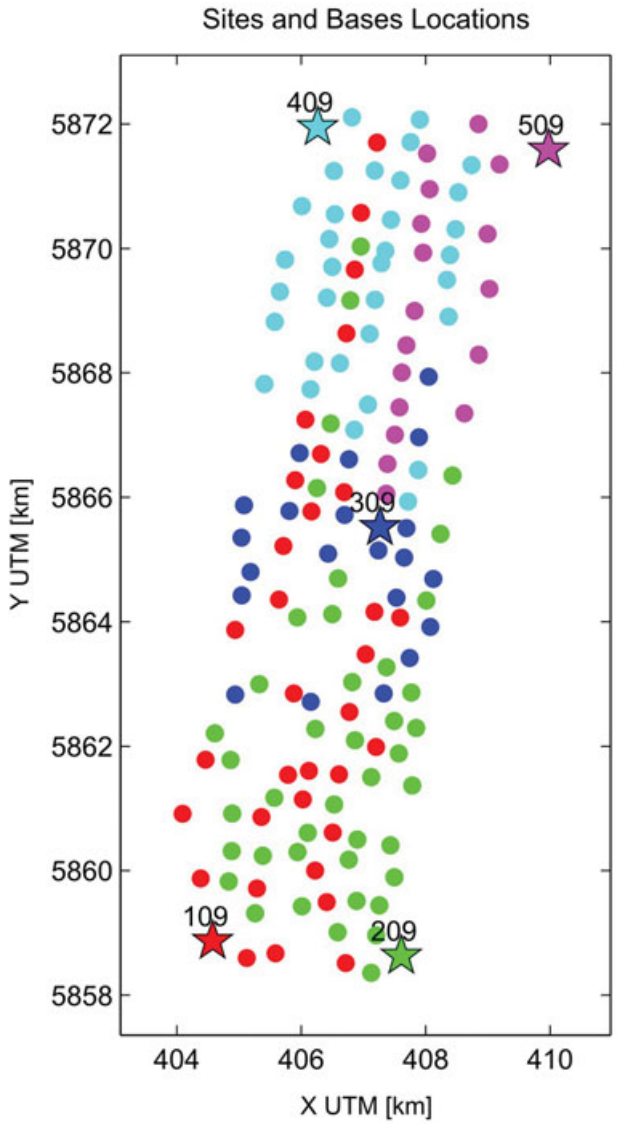

Figure 7 Location map of base (asterisks) and local stations (dots) for the grid around the Groß Schönebeck geothermal test site, located about 40 km north of Berlin (see inset). The local stations are plotted in the same colour as the base station used for pseudo-remote processing. The closest base station producing the smoothest and most unbiased curves was chosen for each local station.

where **C**, the distortion matrix, is a frequency-independent real matrix. By using equations (3) and (9) the observed pseudo-remote impedance tensor can be expressed as:

$$\begin{aligned} Z^{\text{observed}}_{\text{pseudoRR}} &= Z^{\text{observed}}_{L}\mathbf{T}_{\text{B-L}} = \mathbf{C}\mathbf{Z}_{\text{L}}\mathbf{T}_{\text{B-L}} \\ Z^{\text{observed}}_{\text{pseudoRR}} &= \mathbf{C}\mathbf{Z}_{\text{pseudoRR}}, \end{aligned} \tag{10}$$

which is the same relationship as equation (9). Therefore, the pseudo-remote transfer functions estimation is neutral with respect to galvanic distortion, i.e., the transfer functions are affected by galvanic distortion exactly in the same way as the local transfer functions. However, it should be noted that in the presence of strong galvanic distortion, the assumptions used to derive equation (4) are not fulfilled (as the main diagonal components of the impedance tensor can be significantly large) and the correction of the pseudo-remote transfer functions according to equation (4) is not valid.

The pseudo-remote approach can be developed in a remote reference (RR) manner, by inclusion of horizontal magnetic fields of a remote station to reduce bias. For this expanded pseudo-remote/remote approach, we use classical RR processing (Goubau *et al.* 1978; Gamble, Goubau and Clarke 1979). The 'local' site contains electric and vertical magnetic fields measured locally in addition to the horizontal magnetic fields measured at the base station. The experimental setup, demonstrated schematically in Fig. 5, consists in a local station (L), a base station (B) and a remote station (R). Note, the interstation transfer functions between base and local stations ($\mathbf{T}_{\text{B-L}}$) cannot be determined but can be estimated according to equation (8). The ITF between the remote and base stations ($\mathbf{T}_{\text{R-B}}$) becomes part of the remote reference transfer functions calculation. Krings (2007) examined $\mathbf{T}_{\text{R-B}}$ as a possible indicator for data quality and Sokolova, Varentsov and Group (2005) and Ritter *et al.* (1998) and used it as a data rejection criterion for remote reference processing.

CASE STUDY: GROß SCHÖNEBECK GEOTHERMAL TEST SITE

We applied the approach described above to a data set collected in the vicinity of the Groß Schönebeck geothermal test site. The Groß Schönebeck *in situ* geothermal laboratory, located 40 km north of Berlin in north-eastern Germany, is a key site for testing the geothermal potential of deep sedimentary basins. The target reservoir is located in Lower Permian (Rotliegend) sandstones and volcanic strata, which host deep aquifers throughout the north-east German Basin (Huenges, Moeck and the geothermal group of the GF2 2007). The electrical conductivity models shown in Fig. 6 were obtained from MT data along two profiles (Muñoz *et al.* 2010a; Muñoz, Ritter and Moeck 2010b) and indicate shallow sediments with moderate conductivity (~50 Ωm) down to approximately 200 m (A) and a high-conductivity layer (<5 Ωm) with lateral heterogeneities ranging from 1000–3000 m corresponding to Bundsandstein sediments (B). Separated from this layer by a moderate conductivity region associated with Zechstein evaporites, two very high-conductivity anomalies (<1 Ωm) are

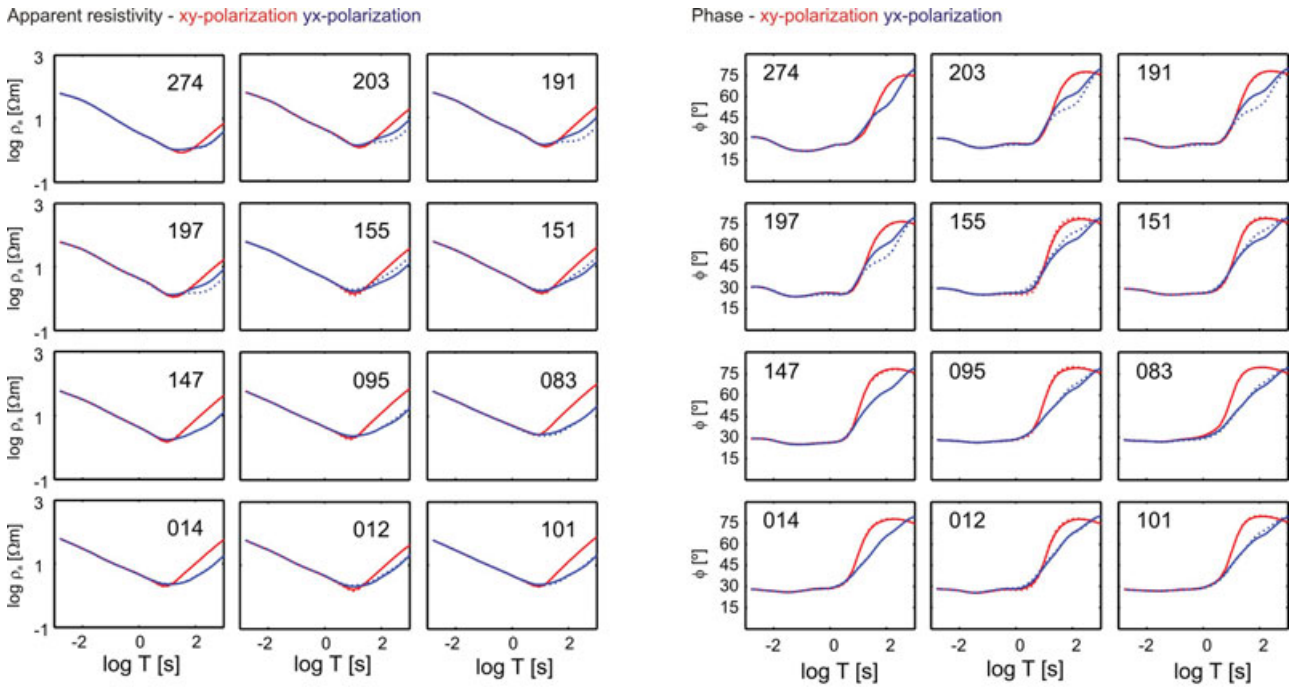

Figure 8 Apparent resistivity and phases curves of a 3D forward modelling study. The 3D model was designed based on the 2D inversion results shown in Fig. 6. The model grid and site distribution resembles the field setup. Solid lines represent local (true) transfer functions and dashed lines the pseudo-remote result using the base stations shown in Fig. 7 for each local station. Differences between local and pseudo-remote results are below 10% for apparent resistivities and 3° for phases. The yx-polarization is more affected than the xy-polarization.

imaged at the reservoir (Rotliegend) level (ca. 4500 m depth) associated with fracturing of the overlaying evaporitic layer (C and D) and below, a high- resistive (>5000 Ωm) basin floor is present (E).

To further investigate the lateral extent of the electrical conductivity features found in the 2D models, an additional grid of 151 stations was measured (Fig. 7). The grid covers an area of approximately 5 km × 25 km and consists in 5 base stations located approximately at the four corners and towards the centre of the study area and 146 local stations with a spacing ranging from 500 m × 500 m to 1000 m × 1000 m. At the base stations two horizontal components of the electric field and three components of the magnetic field were measured as time series in the period range 0.01–1000 s for the whole duration of the experiment (approximately 1 month). At the local stations two horizontal components of the electric field and the vertical component of the magnetic field were measured in the same period range but only for approximately 3 days. In addition, five-component MT data were also measured at a remote reference station located on the island of Rügen in the Baltic Sea (approximately 190 km north of the study area, see Fig. 6). For all the measurements we used the S.P.A.M. MkIII (Ritter *et al*. 1998) and CASTLE systems of the Geophysical Instrument Pool Potsdam and Metronix MFS 05/06 induction coils.

To estimate bias introduced by the pseudo-remote processing approach, we created a 3D grid based on the conductivity models obtained from 2D inversion of the two existing profiles (Muñoz *et al*. 2010b). With 3D forward modelling, the true responses at all local stations can be computed together with the respective pseudo-remote responses, i.e., with reference to any other (base) station on the model grid. A comparison between a (normal) local site and pseudo-remote transfer functions is shown in Figs 8 and 9. The errors introduced by the pseudo-remote reference approach are below 10% for apparent resistivities and 3° for phases for most periods. Further synthetic tests (not shown) indicate that the bias can be reduced if a base station close to the local station is used for pseudo-remote processing. For our field data, however, we found that the closest base station did not always produce the highest quality curves. This is probably due to locally varying noise conditions. In order to reduce the impact of the varying noise conditions, each local station was processed using the pseudo-remote approach with all 5 base stations. The five pseudo-remote transfer functions were compared to determine which combination produced the smoothest, most unbiased

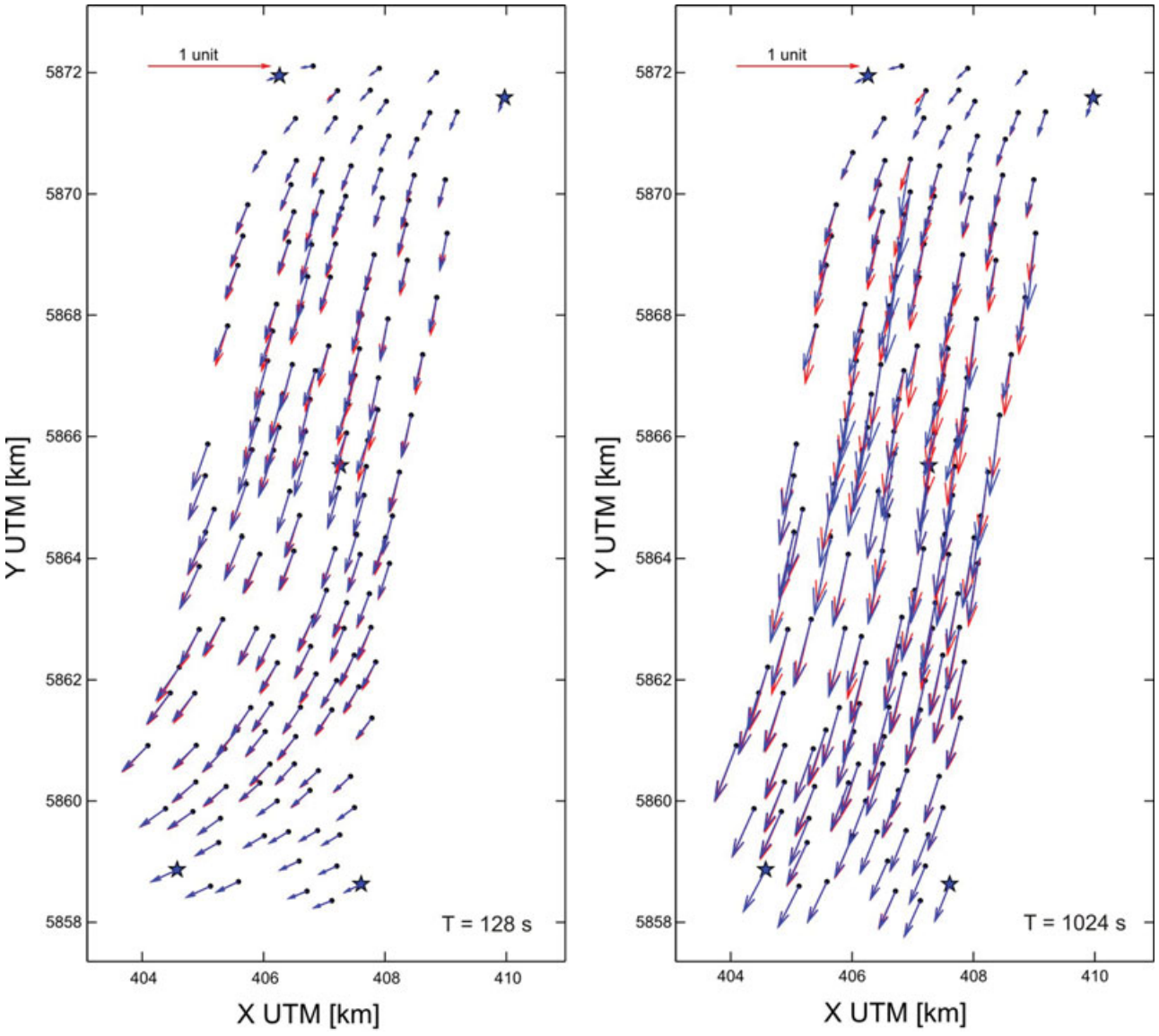

Figure 9 Similar to Fig. 8 but now showing vertical magnetic field transfer functions for two selected periods. The data are presented as induction vectors. The red vectors indicate the local vertical magnetic transfer functions and the blue vectors the pseudo-remote transfer functions using the base stations shown in Fig. 7. The differences between local and pseudo-remote vectors are very small.

curves. In some cases, a possibly higher bias introduced by a more distant base station was accepted if the alternative was more severely scattering curves due to additional noise at the base station. Figure 7 summarizes which base stations were selected to process each of the local stations. Note, we used the same combinations of sites for the 3D modelling study shown in Figs 8 and 9.

Assessing the transfer functions in Fig. 8 reveals that for the xy-polarization, the pseudo-remote approach reproduces the (normal) single site results while the yx-polarization exhibits larger differences. According to equation (4) this indicates that the T_{yy} component of the ITF is closer to unity than the T_{xx} component. This is confirmed by Fig, 10, which shows the measured interstation transfer functions between each pair of base stations. The main diagonal components T_{xx} and T_{yy} are generally close to unity but with T_{xx} showing larger deviations. The off-diagonal components T_{xy} and T_{yx} are close to zero at all periods and for all station pairs. The largest deviations from unity of the ITF are probably caused by noise in the magnetic fields. Figure 11 shows a comparison of ITFs between stations 109–209 measured at two different time intervals. Assuming that the underlying conductivity structure

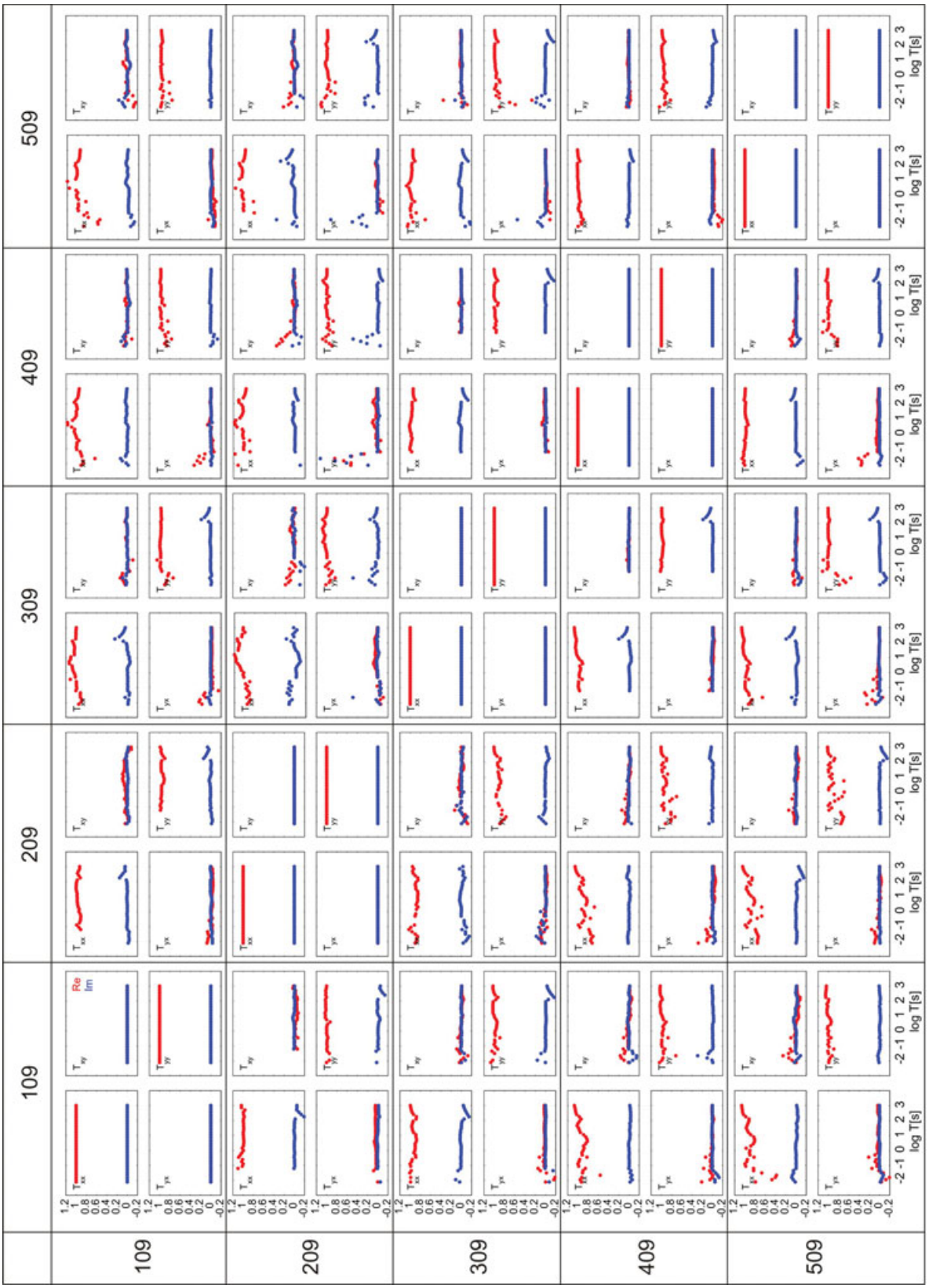

Figure 10 Interstation transfer functions (ITF) between all base station combinations. Red dots represent the real parts and blue dots the imaginary parts. For all base station pairs the ITFs are close to unity (average deviations below 0.1), indicating homogeneous source fields and absence of strong lateral conductivity contrasts.

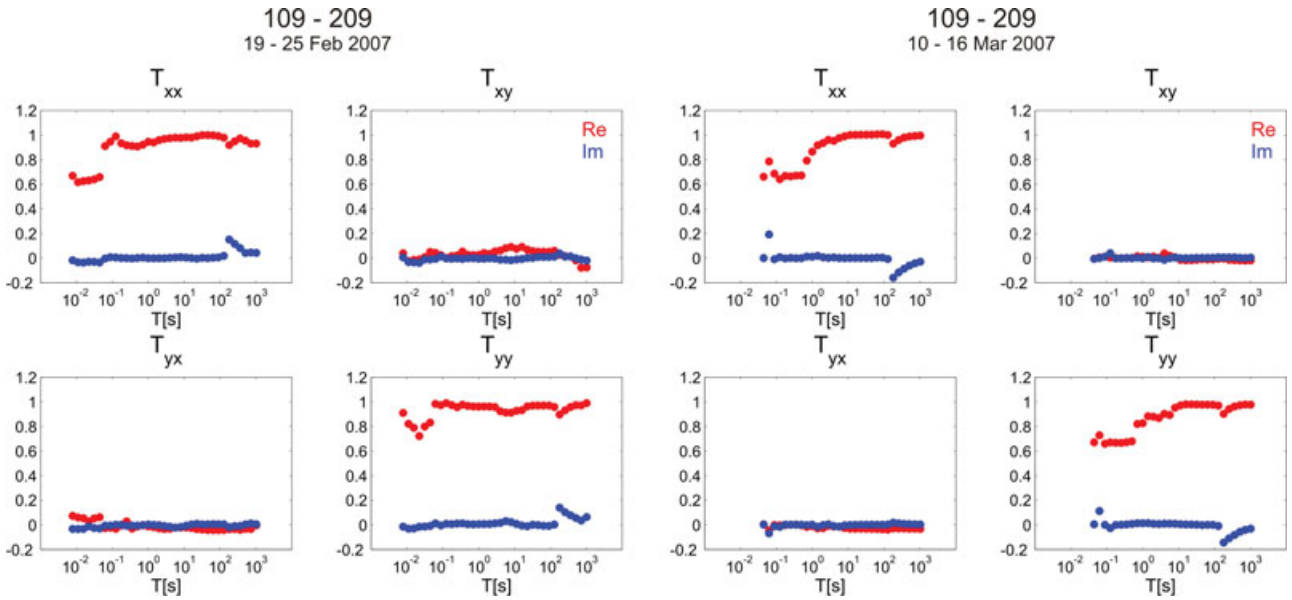

Figure 11 Comparison of the interstation transfer functions between base stations 109–209 measured at two different time windows. Red dots represent the real parts and blue dots the imaginary parts. The differences between the ITFs are caused by varying noise conditions.

does not vary significantly for the duration of the experiment, any changes in the interstation transfer functions must be due to changes in the magnetic fields, either as a source effect or – and more likely – by varying noise conditions.

After choosing an optimum base station for each local site, the data were processed using a hybrid pseudo-remote/remote reference approach using the processing package of Ritter *et al.* (1998) with the modifications of Krings (2007) and Weckmann, Magunia and Ritter (2005). The horizontal magnetic fields of a selected base station were assigned to the local station and this pseudo-station was then processed using the remote reference station on Rügen. Figure 12 shows the apparent resistivity and phase curves for base and local sites. The most obvious outliers were manually removed but nonetheless the curves are rather smooth and consistent, although the populated study area just 40 km north of Berlin is affected by electromagnetic noise (several high-voltage power lines, the Berlin regional trains, etc.). Consistency between apparent resistivity and phase curves was tested using the D+ algorithm (Parker 1980). Figure 13 shows induction vector maps for several selected periods. Despite of some outliers, the overall quality is satisfactory, with induction vectors varying consistently with frequency and in space.

For a preliminary model study of the Groß Schönebeck data set, the MT stations were grouped into four parallel profiles (see Fig. 7). Dimensionality of the impedance tensors was analysed using the algorithm of Becken and Burkhardt (2004). Analysis of sites individually yields strike directions varying in the range 15–25° (with 90° ambiguity), in agreement with the strike direction found by Muñoz *et al.* (2010b). Ellipticities are close to zero and distortion angles are mostly constant in the considered period range for all sites, indicating that the data are consistent with a 2D resistivity structure. The multi-site, multi-period analysis yields a regional strike direction of N68°W (the 90° ambiguity of the strike directions is solved using geological information and the directions of the induction vectors, Fig. 13). The induction vectors, however, do not point exclusively along the profile direction, as would be expected for a 2D resistivity structure.

After rotation of the impedance tensors by −68° and accordingly projection of the induction vectors, the data were inverted using the code of Rodi and Mackie (2001) included in the Winglink software package (www.geosystem.net). Figure 14 shows the 2D resistivity models obtained from inversion of both TE and TM mode apparent resistivity and phases together with the vertical magnetic transfer functions along the four profiles using a value of $\tau = 1$ for the regularization parameter. Error floor settings of 100% for the TE apparent resistivity (i.e., down-weighting this component), 10% for the TM apparent resistivity, 1.5° for the phases and 0.02 for the geomagnetic transfer functions, resulted in root mean squared (RMS) misfits of 2.06, 1.38, 1.76 and 2.15 for the four profiles. Clearly, the main features present in the existing magnetotelluric studies (Fig. 6 and Muñoz *et al.* 2010b) are reproduced in the models. Moderately conductive shallow sediments appear in all four

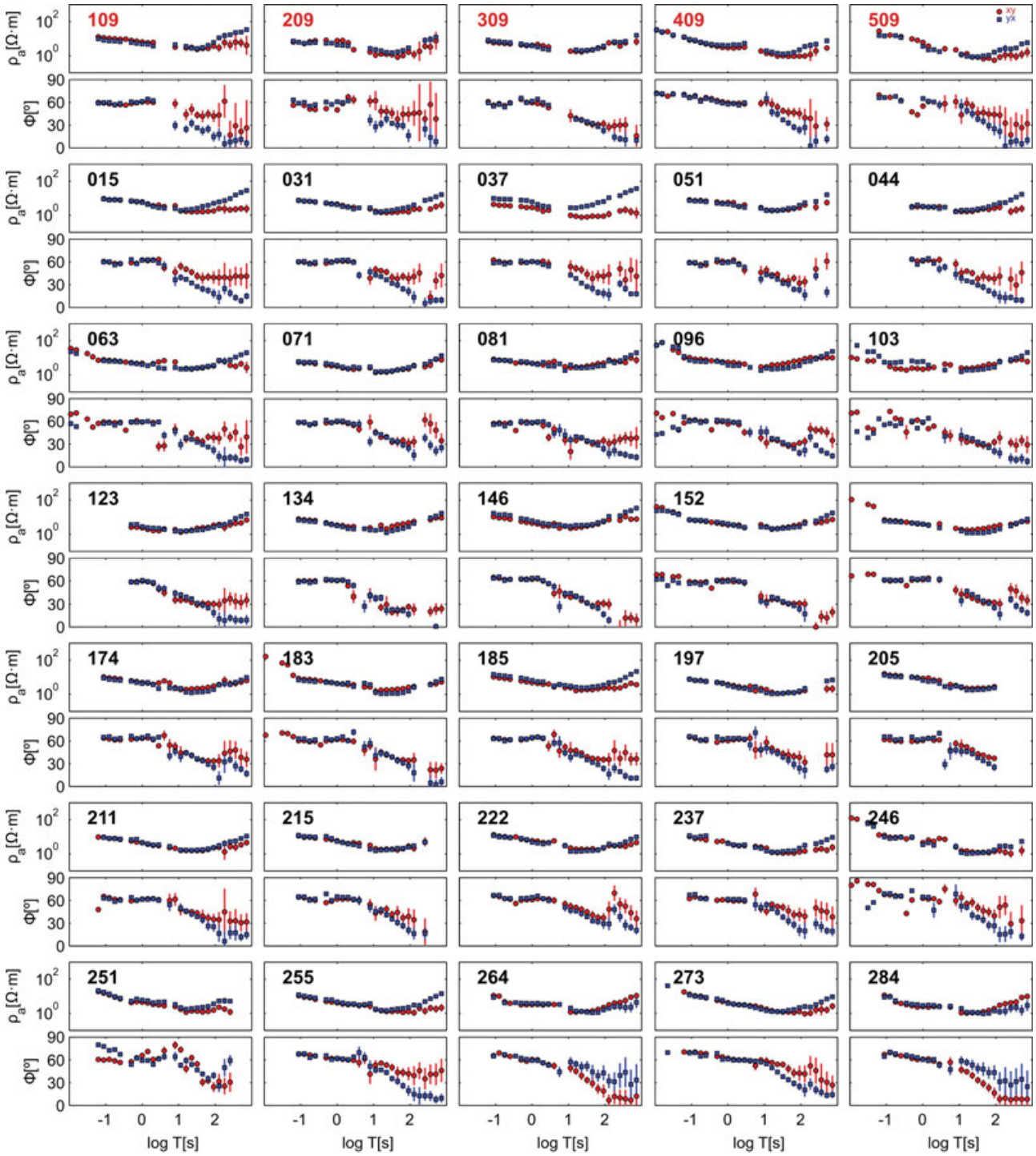

Figure 12 Measured apparent resistivity and phase curves for some exemplary stations. The upper row presents transfer functions of the base stations. Red dots indicate the xy-polarization and blue squares the yx-polarization. The local stations were processed using a hybrid pseudo-remote/remote reference approach. The most severe outliers were removed from the data set for clarity. Although the survey area is affected by electromagnetic noise the data quality is acceptable, with smooth and consistent curves.

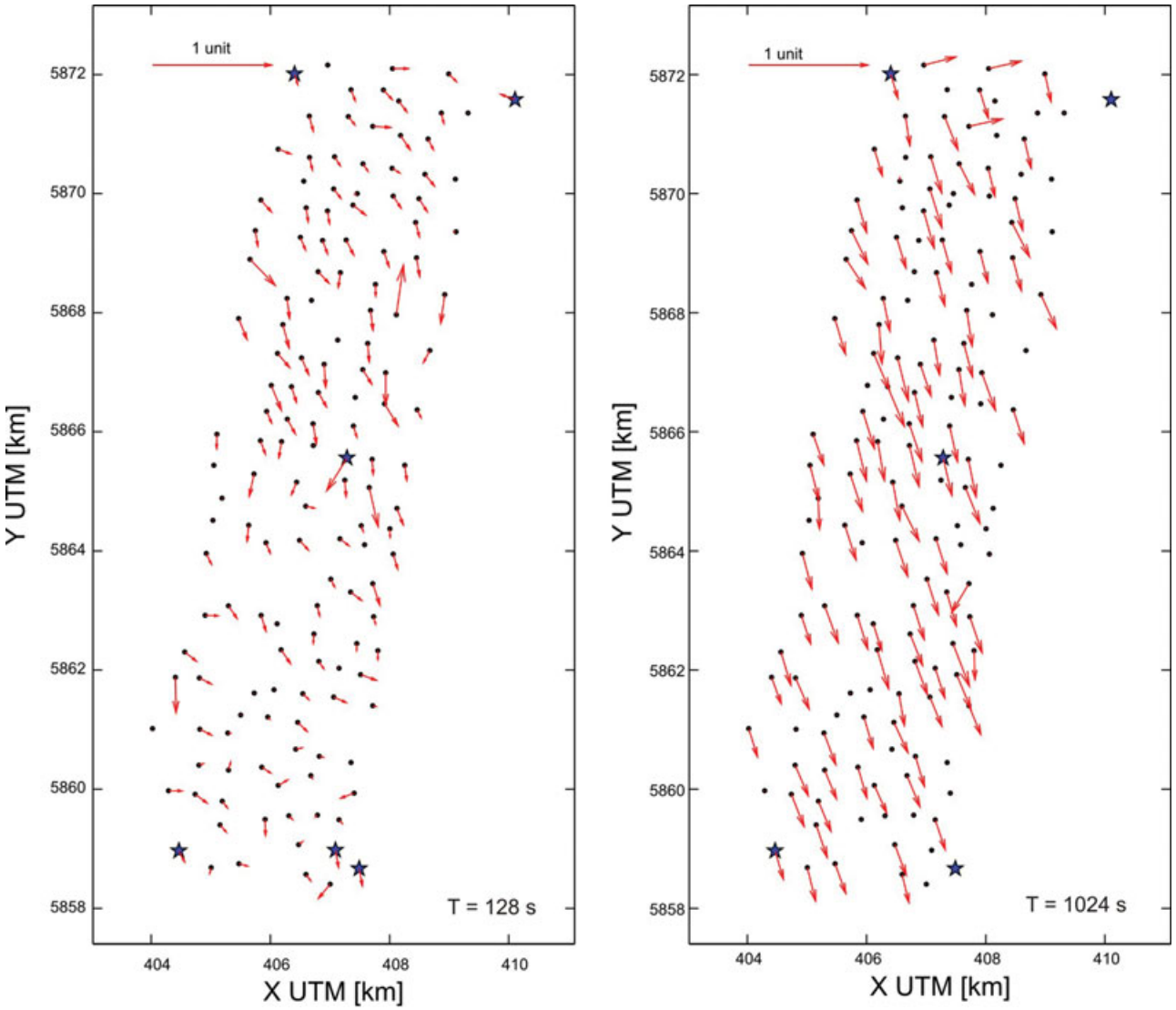

Figure 13 Measured induction vectors for the stations of the measurement grid at periods of 128 s and 1024 s. The stations were processed using a hybrid pseudo-remote/remote reference approach.

profiles as well as high-conductivity layers overlying the Zechstein evaporites and a high-resistivity basin floor. The deeper high-conductivity anomalies (C and D in Fig. 6) also appear in these models but less pronounced. The consistent image across the present four profiles and the previous long profiles suggests a lateral continuation of the conductivity structures along the strike although some 3D effects are present in the data.

CONCLUSIONS AND OUTLOOK

The data acquisition scheme presented here shows promising results as it helps to record a large number of MT stations in a very efficient manner regarding time and resources. The bias introduced by the pseudo-remote approach can be reduced by optimizing the base station locations; locations far from strong conductivity contrasts and homogeneous site distribution over the measurement area are ideal. To further reduce the bias introduced by the pseudo-remote processing technique, we developed and applied a correction scheme that considers the distance of local sites from base stations. Interstation transfer functions (ITF) between pairs of base stations can be examined as quality control and to test the validity of the approach.

Despite fairly high-local noise levels, we managed to retrieve consistent, high-quality impedance tensor estimates and magnetic transfer functions. A remote reference station located far

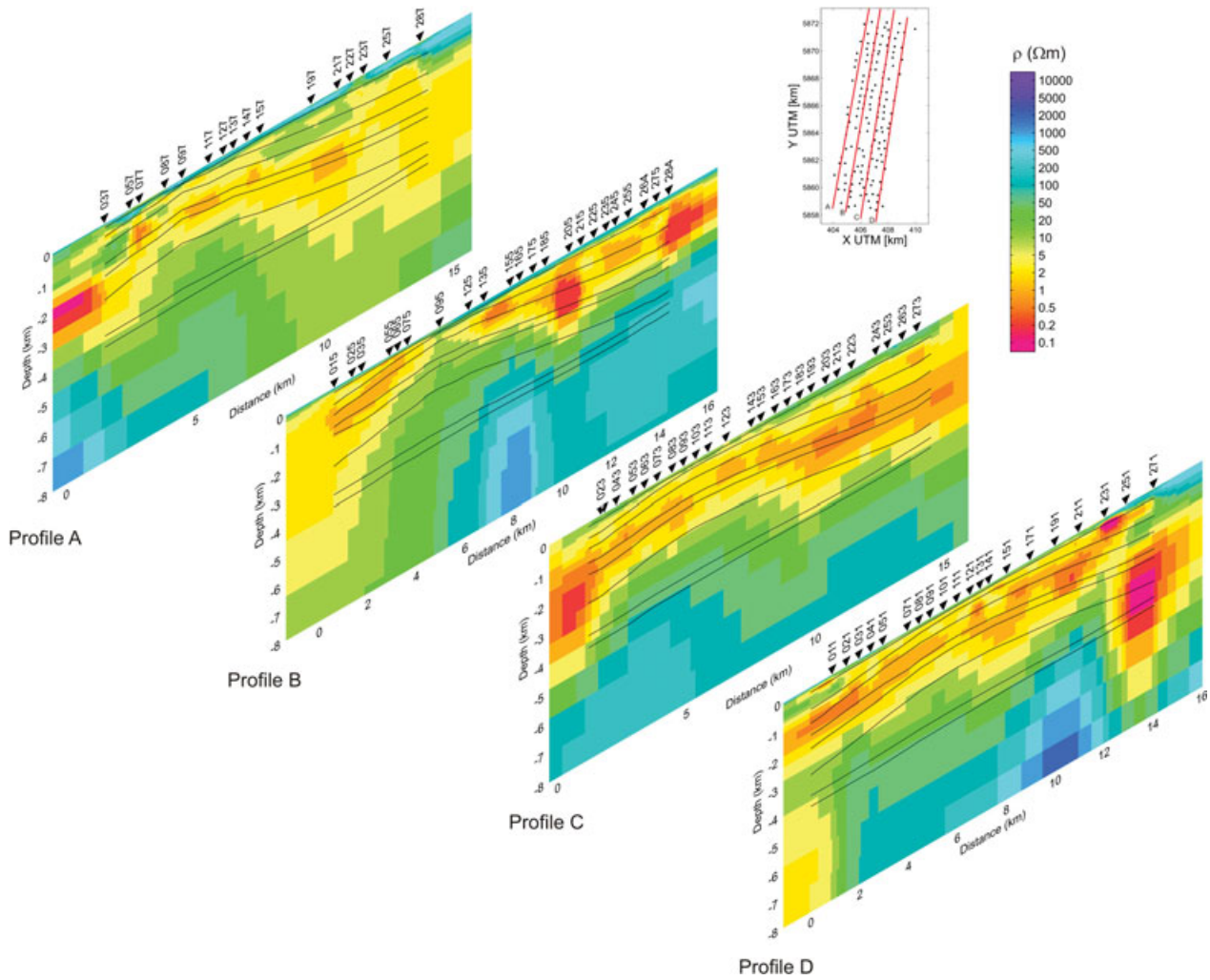

Figure 14 Electrical resistivity models obtained from 2D inversion of the TE and TM modes and the vertical magnetic transfer functions along four parallel profiles A–D. The inverted black triangles show the locations of the stations projected onto the profile lines. Solid black lines represent selected stratigraphic horizons from the geological model of Moeck, Schandelmeier and Holl (2008). The models image moderately resistive sediments to a depth of approximately 200 m, a low-resistivity layer (<5 Ωm) that reproduces the antiform shape produced by the Zechstein evaporites on the overlying sedimentary layers and a high- resistivity (>500 Ωm) basin floor. Deeper low-resistivity regions are found at the reservoir level.

away from the measurement area helped to further improve the data quality. Nevertheless, this pseudo-remote technique is probably most usefully applied to dense station arrays in relatively small survey areas. Care must be taken when applying the presented processing approach to ensure that conditions of homogeneity and coherence of the source fields are not violated, for instance because the survey area is very large or strong anomalies are present. In such cases, errors introduced by the pseudo-remote processing can be significant and can lead to misinterpretations of the data if adequate corrections cannot be applied. As a remedy to this problem, it would be possible to create or modify a 3D inversion code to invert for the pseudo-remote transfer functions instead of the local transfer functions. A similar approach was developed by Soyer and Brasse (2001) to invert interstation transfer functions in 2D.

Further model exploration and a complete 3D inversion of the whole data set are still necessary to fully explain the data and to complete the electrical characterization of the Groß Schönebeck geothermal test site.

ACKNOWLEDGEMENTS

The fieldwork was funded within the 6th Framework Program of the European Union (IGET Project, Contract n° 518378).

The instruments for the magnetotelluric experiments were provided by the Geophysical Instrument Pool Potsdam (GIPP). We thank the comments and suggestions of three anonymous reviewers.

REFERENCES

Becken M. and Burkhardt H. 2004. An ellipticity criterion in magnetotelluric tensor analysis. *Geophysical Journal International* **159**, 69–82.

Egbert G.D. and Kelbert A. 2012. Computational recipes for electromagnetic inverse problems. *Geophysical Journal International* **189**, 251–267.

Gamble T.D., Goubau W.M. and Clarke J. 1979. Magnetotellurics with a remote magnetic reference. *Geophysics* **44**, 53–68.

Garcia X. and Jones A.G. 2005. A new methodology for the acquisition of audio-magnetotelluric (AMT) data in the AMT dead band. *Geophysics* **70**, 119–126.

Goubau W.M., Gamble T.D. and Clarke J. 1978. Magnetotelluric data analysis: Removal of bias. *Geophysics* **43**, 1157–1169.

Huenges E., Moeck I. and the geothermal group of the GFZ 2007. Directional drilling and stimulation of a deep sedimentary geothermal reservoir. *Scientific Drilling* **5**, 47–49.

Krings T. 2007. *The influence of robust statistics, remote reference, and a criterion based on horizontal magnetic transfer functions on MT data processing*. Diploma thesis, WWU Münster – GFZ Potsdam. p.108.

Larsen J.C., Mackie R.L., Manzella A., Fiordelisi A. and Rieven S. 1996. Robust smooth magnetotelluric transfer functions. *Geophysical Journal International* **124**, 801–819.

Mackie R.L., Madden T.R. and Wannamaker P.E. 1993. Three-dimensional magnetotelluric modeling using difference equations – Theory and comparisons to integral equation solutions. *Geophysics* **58**, 215–226.

Mackie R.L., Rodi W. and Watts M.D. 2001. 3-D magnetotelluric inversion for resource exploration. *SEG Expanded Abstracts* **20**, 1501–1504.

Muñoz G., Bauer K., Moeck I., Schulze A. and Ritter O. 2010a. Exploring the Groß Schönebeck (Germany) geothermal site using a statistical joint interpretation of magnetotelluric and seismic tomography models. *Geothermics* **39**, 35–45.

Muñoz G., Ritter O. and Moeck I. 2010b. A target-oriented magnetotelluric inversion approach for characterizing the low enthalpy Groß Schönebeck geothermal reservoir. *Geophysical Journal International* **183**, 1199–1215.

Parker R.L. 1980. The inverse problem of electromagnetic induction: Existence and construction of solutions based on incomplete data. *Journal of Geophysical Research* **85**, 4421–4428.

Ritter O., Junge A. and Dawes G.J.K 1998. New equipment and processing for magnetotelluric remote reference observations. *Geophysical Journal International* **132**, 535–548.

Rodi W. and Mackie R.L. 2001. Nonlinear conjugate gradients algorithm for 2-D magnetotelluric inversion. *Geophysics* **66**, 174–187.

Siripunvaraporn W., Egbert G., Lenbury Y. and Uyeshima M. 2005. Three-dimensional magnetotelluric inversion: Data-space method. *Physics of the Earth and Planetary Interiors* **150**, 3–14.

Sokolova E., Varentsov I. and Group E.P.W. 2005. *RRMC Technique Fights Highly Coherent Noise. 21*. Kolloquium Elektromagnetische Tiefenforschung, eds O. Ritter and H. Brasse.

Torres-Verdin C. and Bostick F.X. 1992. Principles of spatial surface electric field filtering in magnetotellurics: Electromagnetic array profiling (EMAP). *Geophysics* **57**, 603–622.

Weckmann U., Magunia A. and Ritter O. 2005. Effective noise separation for magnetotelluric single site data processing using a frequency domain selection scheme. *Geophysical Journal International* **161**, 456–468.

Zweier R. and Morrison H.F. 1972. Spatial characteristics of mid-latitude geomagnetic micropulsations. *Journal of Geophysical Research* **77**, 674–693.